Calculated and experimental electron energy-loss spectra of La2O3, La(OH)(3), and LaOF nanophases in high permittivity lanthanum-based oxide layers

Lionel Calmels, Pierre-Eugène Coulon, Sylvie Schamm-Chardon

Calculated and experimental electron energy-loss spectra of La_2O_3, $La(OH)_3$, and LaOF nanophases in high permittivity lanthanum-based oxide layers

L. Calmels, P. E. Coulon, and S. Schamm-Chardon

Citation: Appl. Phys. Lett. **98**, 243116 (2011); doi: 10.1063/1.3600783
View online: https://doi.org/10.1063/1.3600783
View Table of Contents: http://aip.scitation.org/toc/apl/98/24
Published by the American Institute of Physics

Calculated and experimental electron energy-loss spectra of La_2O_3, $La(OH)_3$, and LaOF nanophases in high permittivity lanthanum-based oxide layers

L. Calmels,[a] P. E. Coulon, and S. Schamm-Chardon
CEMES-CNRS, Université de Toulouse, 29 rue Jeanne Marvig, BP 94347, F-31055 Toulouse Cedex 4, France

(Received 31 March 2011; accepted 27 May 2011; published online 17 June 2011)

Using first principles methods, the O *K* energy-loss near-edge structure of cubic and hexagonal La_2O_3, $La(OH)_3$, and LaOF phases have been calculated. These calculations support the identification of nanocrystalline phases evidenced experimentally by electron energy-loss spectroscopy (EELS) performed in a transmission electron microscope. The nanocrystals have been observed in atomic layer deposited La_2O_3 thin films developed for advanced metal-oxide-semiconductor field effect transistor applications. The presence of the nanophases can be explained by the hygroscopicity and the particular reactivity with fluorine of La_2O_3. These calculations provide a set of EELS fingerprints which will be useful for local phase identification in La_2O_3-based materials. © *2011 American Institute of Physics*. [doi:10.1063/1.3600783]

An intense research activity is dedicated to reduce the size of electronic devices and in the same time to increase the performances of metal-oxide-semiconductor field effect transistors (MOSFETs). Particularly, the decrease in the gate oxide thickness together with the control of the leakage currents required the introduction of oxides with higher permittivity than classical SiO_2, called high-κ. Hf-based oxides in combination with metal gate electrodes have already been introduced for transistor production into the 45 nm Si complementary metal oxide semiconductor (CMOS) process line.[1] In the same time, rare earth oxides received attention as candidates for sub-45 nm CMOS technology nodes.[2,3] Crystalline La_2O_3 is particularly of concern due to its high κ value ($\sim$27) which is achieved when stabilized with the hexagonal $P63/mmc$ structure.[4,5] However, this oxide is the most reactive of the lanthanide series because hygroscopicity[6] associated with the lanthanide contraction phenomenon[2] impedes the formation of a stable hexagonal La_2O_3 phase as this quickly relaxes upon air exposure to monoclinic LaO(OH) and hexagonal $La(OH)_3$.[5,7–9] Moreover, the lanthanide contraction phenomenon impairs also the La_2O_3 thermal stability on Si, giving rise during growth and postdeposition annealing to Si diffusion into La_2O_3 (Ref. 10) and to the formation of an amorphous lanthanum silicate interfacial layer.[11] Instability of La_2O_3 against CO_2 has also been described leading to disordered oxy- and hydroxyl-carbonate phases.[12–14] Nanophases of most of the La-based compounds listed above can be observed in ultrathin La-based oxide layers prepared by atomic layer deposition (ALD) and developed for CMOS applications.[9] In addition, we evidenced La_2O_3 reactivity against fluorine.

Electron energy-loss spectroscopy (EELS) performed in a transmission electron microscope (TEM) with a nanometer sized probe is the relevant tool to both image and analyze nanophases. EELS is useful when conventional diffraction methods or high resolution imaging are not sufficient to conclude on the atomic structure of a nanophase. In particular, features and details appearing as fine structure at the oxygen *K*-edge (O *K*) called energy-loss near-edge structure (ELNES) will be different for O atoms engaged in different phases corresponding to different neighbors configurations. Indeed, ELNES provides information on the contribution of oxygen *p* orbitals to unoccupied states because electronic transitions involved in this excitation edge from the oxygen 1*s* core-level to unoccupied valence states obey the electric dipole selection rules.[15]

In this letter, we focus on the calculation of O *K* ELNES and the comparison to experimental data for nanocrystalline phases that can be detected within ALD prepared La- and O-based thin films.[9,11] Based on the cross-correlation of high resolution images, electron diffraction patterns, and chemical analyses, we decided to calculate O *K* ELNES for hexagonal $La(OH)_3$, cubic (*c*-) and hexagonal (*h*-) La_2O_3, cubic, trigonal, and tetragonal LaOF to interpret our experimental data. C-containing phases being amorphous were not considered. For noncubic crystals, the calculated spectra are spherically averaged over the direction of the momentum transfer; this is justified because the corresponding experimental spectra usually include contributions from several randomly oriented nanocrystals. Few literature data exists for La-based hydroxide, oxide, and oxyfluoride O *K* ELNES. O *K* for polycrystalline La_2O_3 is shown in Ref. 16 with no indication of the phase analyzed. The only work that discusses O *K* ELNES of rare earth sesquioxides, among them *h*-La_2O_3, was on the basis of fine structure obtained a long time ago with limited energy resolution.[17] No data are available concerning the O *K* ELNES of $La(OH)_3$ and LaOF phases. We propose *ab initio* calculated O *K* ELNES of La-based oxides. The calculations were performed with the code FEFF8, which is based on the density functional theory and uses a self-consistent real-space multiple-scattering approach.[18] Clusters of atoms with more than 200 atoms and a spherical harmonic basis with maximum angular momentum $l_{max}=3$ were typically used. Core-hole effects were taken into account and a 0.7 eV broadening has been used. The calculated ELNES have been compared to spectra acquired on nanocrystals imaged in lan-

[a]Electronic mail: lionel.calmels@cemes.fr.

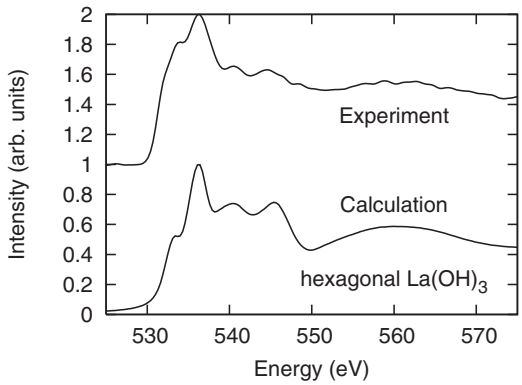

FIG. 1. Electron ELNES at the oxygen *K*-edge for lanthanum hydroxide $La(OH)_3$. The upper and lower curves, respectively, describe the experimental and the calculated spectra. The spectra have been normalized to the most intense fine structure near the edge onset.

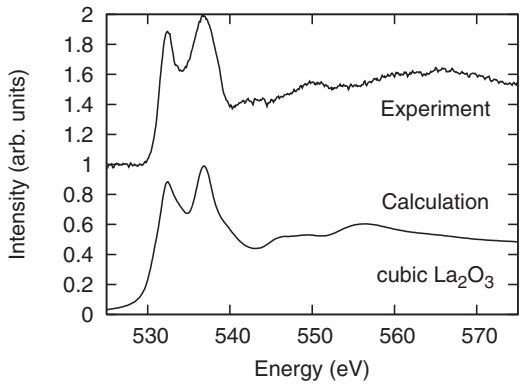

FIG. 2. Same as in Fig. 1 for the cubic phase of lanthanum oxide La_2O_3.

thanum oxide-based films, with a FEI Tecnai F20 TEM operating at 200 kV, equipped with a field emission gun, an objective lens corrected for spherical aberrations (CEOS) and a Gatan Imaging Filter (TRIDIEM). The energy resolution of the experiments is close to 1 eV.

Typically, the experimental O *K* fine structure in as-grown films shown in Fig. 1 (top) corresponds to the lowest La/O stoichiometry, around 0.3. In this case, the electron diffraction pattern was clearly associated with the hexagonal $La(OH)_3$ phase but the EELS analysis revealed the presence of carbon in addition to lanthanum and oxygen. The features of the calculated ELNES for the hexagonal structure of lanthanum hydroxide $La(OH)_3$ with space group $P63/m$ (Ref. 19) shown in Fig. 1 (bottom) are at the same energies than the experimental ones, even if the relative height of the peaks and shoulders is slightly different. It consists in a first broadened structure for energy losses between 532 and 550 eV, with a small shoulder at 533 eV and a higher peak at 536 eV, and two smaller peaks near 540 and 546 eV. This broadened structure is followed by a large distribution between 550 and 570 eV, with a maximum intensity around 560 eV. The energy region between 530 and 535 eV is more intense in the experimental ELNES. This difference could be attributed to the added signature of O atoms engaged in amorphous oxy- and hydroxyl-carbonates that are generally present at the surfaces of crystalline $La(OH)_3$;[12–14] it could also originate from the dependence of the EELS spectra on the electron beam energy, illuminating and collection angle not taken into account in our calculations. After a relevant vacuum annealing procedure, it is possible to obtain the La_2O_3 phase.[4,5,9] Determination of the La/O stoichiometry is not sufficient to distinguish between *c*-La_2O_3 and *h*-La_2O_3. Therefore, we concentrate our effort on the identification of these nanophases from their O *K* ELNES. The fine structure of *c*-La_2O_3 with $Ia\text{-}3$ space group[20] and of *h*-La_2O_3 with $P63/mmc$ space group[21–23] was calculated. For *c*-La_2O_3, two intense peaks with similar intensities at 532.4 and 536.8 eV that reflect the hybridization of unoccupied oxygen *p* with lanthanum e_g and t_{2g} orbitals splitted by the crystal field[24] are followed by a plateau with smooth oscillations (Fig. 2 bottom). The calculation of the fine structure at the O *K* edge for *h*-La_2O_3 is more difficult, the unit cell of *h*-La_2O_3 containing two nonequivalent oxygen atoms. The spectra calculated for each of these two atoms must be added to get the ELNES of the whole crystal, keeping in mind that the edge onset may not be exactly at the same energy for the two oxygen atoms. The code FEFF8 is reliable to calculate the ELNES of a given atom (correct number of peaks and energy intervals between these peaks). Unfortunately, this code does not calculate the edge onset accurately and cannot give access to the energy shift between the edge onsets of the two nonequivalent oxygen atoms. We used the *ab initio* code WIEN2K (Ref. 25) to estimate this shift: for each of the two nonequivalent oxygen atoms, we calculated the energy difference between the 1*s* core level and the lowest unoccupied energy band which involves *p* atomic orbitals of this atom. This energy difference is greater for one of the oxygen atoms, leading to a 2.47 eV shift between the edge onsets. The whole spectrum calculated for *h*-La_2O_3 is shown in Fig. 3. It contains a main broadened peak between 530 and 540 eV, followed by a rather flat plateau. The broadened peak contains four small oscillations, each of the nonequivalent oxygen atoms being responsible for the existence of two distinct peaks with intensities and widths which differ from those calculated for *c*-La_2O_3, the crystal field being different. The calculated *c*-La_2O_3 is comparable to experimental data acquired on $La(OH)_3$ ALD thick films annealed at temperatures between 300 and 500 °C (Ref. 5) or transformed under the intense electron beam of a field emission source TEM. The calculated *h*-La_2O_3 can be compared to the experimental one of a dedicated sample (Fig. 3). Indeed, due to the particular high hygroscopicity of *h*-La_2O_3, it was difficult to stabilize this phase without taking precautions. Particularly, even if this phase was evidenced by x-ray analyses in ALD thin films (20 nm) annealed under vacuum at 600 °C,[9] it was impos-

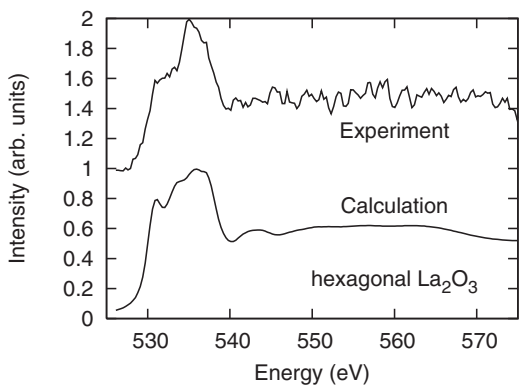

FIG. 3. Same as in Fig. 1 for the hexagonal phase of lanthanum oxide La_2O_3.

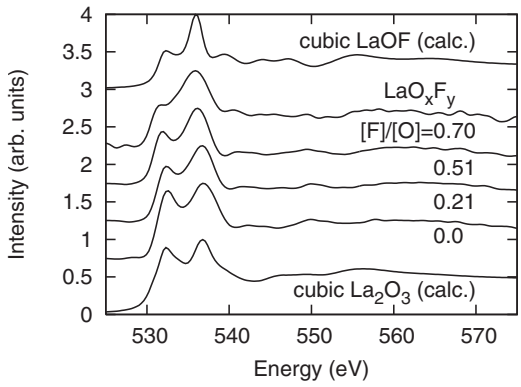

FIG. 4. EELS spectra measured at the oxygen *K*-edge of lanthanum oxyfluorides LaO_xF_y with different chemical compositions. The experimental data obtained for samples with [F]/[O]=0.7, 0.51, 0.21, and 0.0 are compared to the spectra calculated for cubic LaOF (upper curve in the figure) and cubic La_2O_3 (lower curve in the figure).

sible to observe it in the corresponding TEM prepared samples. We only succeeded in observing *h*-La_2O_3 by electron diffraction and EELS in TEM slab prepared from dedicated La_2O_3 film that were deposited by e-beam and sandwiched *in situ* between two silica layers after being annealed at 800 °C.

Presence of fluorine was detected in the analyzed films, particularly in the annealed ones together with *c*- and *h*-La_2O_3. Fluorine incorporation in high permittivity oxides is well studied for semiconductor surface passivation and for improvement of electrical performances, see, for example, Refs. 26 and 27 but the effect of fluorine incorporation in bulk and thin La_2O_3 films has not yet been reported. From our TEM experiments, we suspect that fluorine was present in the as-grown films evenly dispersed and that under the intense electron beam of field emission source TEM some reactivity occurs inducing the formation of lanthanum oxyfluoride, LaOF. LaOF can exist with the tetragonal (space group $P4/nmm$),[28] trigonal (R-$3m$),[28] or cubic (Fm-$3m$) structure.[29] The calculated O *K* ELNES is rather similar for all these phases (only *c*-LaOF is shown in Fig. 4), with a first peak near 532 eV and a second peak which corresponds to the maximum of intensity near 537 eV. Smaller peaks follow, which are found at the same energies for the three crystal structures. The experimental EELS spectrum measured on nanocrystals with different fluorine contents ([F]/[O]=0.7,0.51,0.21,0.0) are shown in Fig. 4 together with the reference *c*-La_2O_3. The same trend is observed in all the experimental data, with two important energy loss peaks with maxima at energies similar to the ones calculated for the LaOF phases. The second of these two peaks increases at the expense of the first one when the fluorine content increases, in agreement with the calculated spectra. The spectra calculated for cubic La_2O_3 and LaOF have different fine structures and can be used as fingerprints for the identification of these two phases which, otherwise, could not be distinguished by diffraction methods because of vicinal diffracting planes.[20,29]

In conclusion, we used *ab initio* methods to calculate the fine structure of the EELS spectra at the oxygen *K*-edge of hexagonal La_2O_3, cubic La_2O_3, hexagonal $La(OH)_3$, tetragonal, trigonal, and cubic LaOF. The calculated spectra, which clearly have a different fine structure, have been compared to experimental data measured by EELS in a TEM on ALD grown La-based films. These results can be used as a set of fingerprints which could help to identify the atomic structures of nanocrystals which can be found in lanthanum-based materials as illustrated here for high-κ gate thin films.

Calculations have been performed at the CALMIP/UPS Toulouse parallel computer center. Part of this work was support by the European FP6-Program "REALISE" (Grant No. IST-NMP 016172), Luca Lamagna providing the ALD samples, and Mircea Modreanu the e-beam sample.

[1]M. Bohr, R. Chau, T. Ghani, and K. Mistry, IEEE Spectrum **44**, 29 (2007).
[2]*Rare Earth Oxide Thin Films: Growth, Characterization, and Applications*, Topics in Applied Physics Vol. 106, edited by M. Fanciulli and G. Scarel (Springer, Berlin, 2007), pp. 1–14.
[3]J. Robertson, J. Appl. Phys. **104**, 124111 (2008).
[4]G. Scarel, A. Debernardi, D. Tsoutsou, S. Spiga, S. C. Capelli, L. Lamagna, S. N. Volkos, M. Alia, and M. Fanciulli, Appl. Phys. Lett. **91**, 102901 (2007).
[5]D. Tsoutsou, G. Scarel, A. Debernardi, S. C. Capelli, S. N. Volkos, L. Lamagna, S. Schamm, P. E. Coulon, and M. Fanciulli, Microelectron. Eng. **85**, 2411 (2008).
[6]S. Jeon and H. Hwang, J. Appl. Phys. **93**, 6393 (2003).
[7]M. Nieminen, M. Putkonen, and L. Niinistö, Appl. Surf. Sci. **174**, 155 (2001).
[8]Y. Zhao, M. Toyama, K. Kita, K. Kyuno, and A. Toriumi, Appl. Phys. Lett. **88**, 072904 (2006).
[9]L. Lamagna, C. Wiemer, M. Perego, S. N. Volkos, S. Baldovino, D. Tsoutsou, S. Schamm-Chardon, P. E. Coulon, and M. Fanciulli, J. Appl. Phys. **108**, 084108 (2010).
[10]H. Ono and T. Katsumata, Appl. Phys. Lett. **78**, 1832 (2001).
[11]S. Schamm, P. E. Coulon, S. Miao, S. N. Volkos, L. H. Lu, L. Lamagna, C. Wiemer, D. Tsoutsou, G. Scarel, and M. Fanciulli, J. Electrochem. Soc. **156**, H1 (2009).
[12]S. Bernal, G. Blanco, J. M. Gatica, J. A. Pérez Omil, J. M. Pintado, and H. Vidal, in *Binary Rare Earth Oxides*, edited by G. A. Adachi, N. Imanaka, and Z. Kang (Kluwer Academic, Springer, 2004), Chap. 2, p. 9.
[13]S. Bernal, G. Blanco, J. J. Calvino, J. A. Pérez Omil, and J. M. Pintado, J. Alloys Compd. **408–412**, 496 (2006).
[14]T. Gougousi and G. N. Parsons, J. Appl. Phys. **95**, 1391 (2004).
[15]R. F. Egerton, *Electron Energy Loss Spectroscopy in the Electron Microscope* (Plenum Press, New York, 1996).
[16]M. Gao, L. M. Peng, X. L. Dong, B. R. Zhao, G. D. Liu, and Z. X. Zhao, Phys. Rev. B **62**, 5413 (2000).
[17]L. M. Brown, C. Colliex, and M. Gasgnier, J. Phys. Colloq. **45**, C2-433 (1984).
[18]A. L. Ankudinov, B. Ravel, J. J. Rehr, and S. D. Conradson, Phys. Rev. B **58**, 7565 (1998).
[19]G. W. Beall, W. O. Milligan, and H. A. Wolcott, J. Inorg. Nucl. Chem. **39**, 65 (1977).
[20]N. Hirosaki, S. Ogata, and C. Kocer, J. Alloys Compd. **351**, 31 (2003).
[21]L. Petit, A. Svane, Z. Szotek, and W. M. Temmerman, Phys. Rev. B **72**, 205118 (2005).
[22]G. V. Samsonov and I. Y. Gil'man, Sov. Powder Metall. Met. Ceram **13**, 925 (1974).
[23]Hk. Muller-Buschbaum and H. G. V. Schenering, Z. Anorg. Allg. Chem. **340**, 232 (1965).
[24]S.-G. Lim, S. Kriventsov, T. Jackson, J. H. Haeni, D. G. Schlom, A. M. Balbashov, R. Uecker, P. Reiche, J. L. Freeouf, and G. Lucovsky, J. Appl. Phys. **91**, 4500 (2002).
[25]P. Blaha, K. Schwarz, G. K. H. Madsen, D. Kvasnicka, and J. Luitz, *WIEN2K, an Augmented Plane Wave Plus Local Orbitals Program for Calculating Crystal Properties* (Vienna University of Technology, Vienna, 2001).
[26]C. X. Li, C. H. Leung, P. T. Lai, and J. P. Xu, Solid-State Electron. **54**, 675 (2010).
[27]C. R. Hsieh, Y. Y. Chen, K. W. Lu, G. Lin, and J. C. Lou, IEEE Electron Device Lett. **31**, 1446 (2010).
[28]W. H. Zachariasen, Acta Crystallogr. **4**, 231 (1951).
[29]W. Klein and H. A. Klein, Z. Anorg. Allg. Chem. **248**, 167 (1941).